Weak coupling Josephson junction as a current probe: effect of dissipation on escape dynamics

J.M. Kivioja†, T.E. Nieminen†, J. Claudon‡, O. Buisson‡, F.W.J. Hekking§, J.P. Pekola†

†Low Temperature Laboratory, Helsinki University of Technology, P.O. Box 3500, 02015 HUT, Finland

‡Centre de Recherches sur les Très Basses Températures, laboratoire associé à l'Université Joseph Fourier, C.N.R.S., BP 166, 38042 Grenoble-cedex 9, France

§Laboratoire de Physique et Modélisation des Milieux Condensés, C.N.R.S. and Université Joseph Fourier, B.P. 166, 38042 Grenoble Cedex 9, France

Abstract.

We have studied the temperature dependence of escape phenomena in various underdamped Josephson junctions. The junctions had different Josephson coupling energies E_J which were relatively small, but larger than the charging energy E_C. Upon increasing temperature T, we first observe the usual crossover between macroscopic quantum tunnelling and thermally activated (TA) behavior at temperatures $k_BT \sim \hbar\omega_p$, where ω_p is the plasma frequency of the junction. Increasing T further, the width of the switching current distribution has, counter-intuitively, a non-monotonic temperature dependence. This can be explained by the novel cross-over from TA behavior to underdamped phase diffusion. We show that this cross-over is expected to occur at temperatures such that $k_BT \sim E_J(1-4/\pi Q)^3/2$, where Q is the quality factor of the junction at the plasma frequency, in agreement with experiment. Our findings can be compared with detailed model calculations which take into account dissipation and level quantization in a metastable well.

Particular attention is paid to the sample with the smallest E_J, which shows extensive phase diffusion even at the lowest temperatures. This sample consists of a dc-SQUID and a single Josephson junction close to each other, such that the SQUID acts as a tunable inductive protection for the single junction from fluctuations of a dissipative environment. By varying the flux through the dc-SQUID we present, for the first time, experimental evidence of the escape of a Josephson junction from the phase diffusion regime to the free running state in a tunable environment. We also show that in the zero voltage state the losses mainly occur at frequencies near the plasma resonance.

Submitted to: *New J. Phys.*

PACS numbers: 74.50.+r, 85.35.-p,85.25.Dq

Contents

1. Introduction

In quantum computing one needs, besides a quantum bit, also a way to measure the quantum state of the system. Recently in many superconducting quantum bit experiments the hysteretic Josephson junction (JJ) escaping from its zero voltage state has successfully been used in the detection of the quantum state [1, 2]. In these applications a hysteretic JJ is also providing inductive protection against phase fluctuations. Escape measurements also enable one to perform conventional large bandwidth current measurements with extensive statistical averaging, and recently there have been proposals to use escape measurements as classical ammeters for studying phenomena like shot-noise [3, 4, 5]. For many purposes it may be advantageous to reduce the critical current I_c of the detecting junction in order to increase the measurement sensivity. Yet the physics governing escape phenomena of small I_c junctions, *i.e.*, junctions where the thermal energy k_BT is of the order of the Josephson coupling energy $E_J = \frac{\hbar}{2e}I_c$, ultimately differs from those with larger I_c, and this sets a limit on how far one can reduce I_c still maintaining the useful features of the detector [6, 7, 8]. In the present work we have investigated experimentally in this limit the phase dynamics in

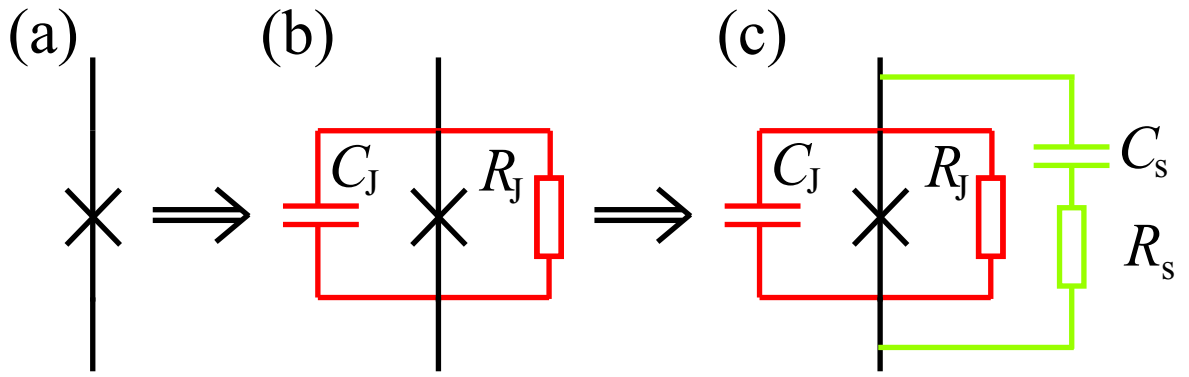

Figure 1. In the RCSJ-model the real Josephson junction (a) is modeled by an ideal junction, which has capacitance and dissipative shunting impedance in parallel (b). Normally the dissipative environment is strongly frequency dependent and the model presented in Fig. (c) is more realistic.

underdamped Josephson junctions and dc SQUIDs. Studied samples were either in the weak Josephson coupling regime with small I_c or in the intermediate regime between "standard" strong coupling junctions ($E_J \gg k_B T$) and the junctions with weak coupling. We will see that in this intermediate regime the usual escape from a single metastable state and the underdamped phase diffusion both play a role.

2. Josephson junction

2.1. RCSJ-model

Josephson junction is a weak link (*e.g.* tunnel junction) between two superconducting electrodes. It can be characterized by its coupling energy $E_J = \frac{\Phi_0}{2\pi} I_c$, charging energy $E_C = e^2/2C_J$, and dissipation $R(\omega) = 1/Re\ \{Y(\omega)\}$. Here C_J is the capacitance of the junction and $\Phi_0 = h/2e$ is the flux quantum. The dynamics of a JJ can be described by the resistively and capacitively shunted junction model (RSCJ) presented in Fig. 1 (b). In this model the junction capacitance and dissipative resistor are in parallel with an ideal Josephson junction. This leads to the model where a fictive phase particle of mass $m = \hbar^2/8E_C$ whose position is given by the difference of the superconducting phase of the junction, φ, resides in a tilted cosine potential $U(\varphi) = -E_J\ (\cos\varphi + I/I_c\ \varphi)$ schematically presented in Fig. 2. The motion of φ is also affected by viscous drag $(\frac{\hbar}{2e})^2\ 1/R(\omega)\ \frac{d\varphi}{dt} = \frac{E_J}{\omega_p Q}\frac{d\varphi}{dt}$ [9]. Here $Q(\omega) = \omega_p R(\omega) C_J$ is the quality factor of the junction, and $\omega_p = \sqrt{\frac{d^2U/d\varphi^2}{m}} = \omega_p^0\ q_0^{1/2} = \frac{1}{\hbar}\sqrt{8E_J E_C}\ q_0^{1/2}$ is the plasma frequency, *i.e.*, the angular frequency of small oscillations around the metastable minimum of the potential and $q_0 \cong \sqrt{2(1 - I/I_c)}$ at currents close to I_c (ω_p^0 is the plasma frequency at zero bias). When the biasing current is close to the critical value, the potential is well approximated by the cubic form $U(q) = 3\ \Delta U\ (q/q_0)^2(1 - \frac{2}{3}q/q_0)$, where $q = \varphi/2 - \frac{\pi}{4} + \frac{1}{2}q_0$, and $\Delta U = \frac{2}{3}\ E_J\ q_0^3$ is the height of the potential barrier.

The dynamics of the Josephson junction can be either overdamped ($Q < 1$) or underdamped ($Q > 1$). In the underdamped dynamics the IV-characteristic of the junction is hysteretic: with increasing current the voltage will jump abruptly from zero to $V \approx 2\Delta_{BCS}/e$ at $I = I_{sw} < I_c$. Here Δ_{BCS} is the superconducting gap. On the contrary, in the case $Q < 1$ the IV-characteristic is non-hysteretic and the voltage increases continuously.

2.2. The dynamics of the underdamped Josephson junction

Figure 2 presents schematically the dynamics of a hysteretic Josephson junction. The upper inset shows an example of a measured IV-characteristic and in the main frame we present the corresponding dynamics of the phase particle in the tilted cosine potential. There are two distinguishable states of the system: the superconducting S-state and the high voltage N-state. In the first one the phase has constant average value and the voltage across the junction is close to zero. With increasing current the phase particle will *escape* from the metastable S-state and switch to the second state, where the phase is running freely. In this N-state the voltage is about twice the superconducting gap ($2\Delta_{BCS} \approx 360\,\mu$V for aluminum). Escape is fully a stochastic phenomenon and the value of the switching current changes from current sweep to another. With decreasing current, the dissipation is slowing down the phase particle and at $I = I_r$ it will be relocalized again to the S-state. This *retrapping* current I_r differs from that of escaping and it strongly depends on dissipation.

Phase particle can escape from a metastable well in the S-state either via thermal activation (TA) over, or quantum tunnelling (MQT) through the barrier. For strong coupling junctions ($\hbar\omega_p \ll \Delta U$) we can assume that there is a continuum of levels within a metastable potential well, which leads to the thermal activation rate

$$\Gamma_{TA} = a_t \frac{\omega_p}{2\pi}\, e^{-\frac{\Delta U}{k_B T}}, \tag{1}$$

where ΔU is the height of the potential barrier [10] and a_t is the dissipation dependent prefactor, which is of the order of unity with typical experimental parameters [11]. The tunnelling rate out of the bottom of the potential well can be calculated using standard WKB approximations leading to [10]

$$\Gamma_{MQT} = a_{MQT} \frac{\omega_p}{2\pi} e^{-B}. \tag{2}$$

where $a_{MQT} = A_0\,[1 + 2.86\alpha + O(\alpha^2)]$ with $A_0 = 12\sqrt{6\pi}\sqrt{\frac{\Delta U}{\hbar\omega_p}}$ and $B = B_0\,[1 + 1.74\alpha + O(\alpha^2)]$ with $B_0 = \frac{36}{5}\frac{\Delta U}{\hbar\omega_p}$ [12, 13]. The dissipation is described by $\alpha = 1/2Q$. The total escape rate can be approximated by $\Gamma_{TOT}(I) \simeq \Gamma_{MQT}(I) + \Gamma_{TA}(I)$ and the total escape probability in the time interval $0 \le t \le \tau$ can be written as $P = 1 - e^{-\int_0^\tau \Gamma_{TOT}[I(t)]dt}$.

The two conventional methods to investigate escape dynamics are as follows: 1. by ramping biasing current through the junction and by measuring the distribution of the switching currents, or 2. by measuring escape rate directly at different values of the bias current. Escape rates per unit time can be determined via the escape

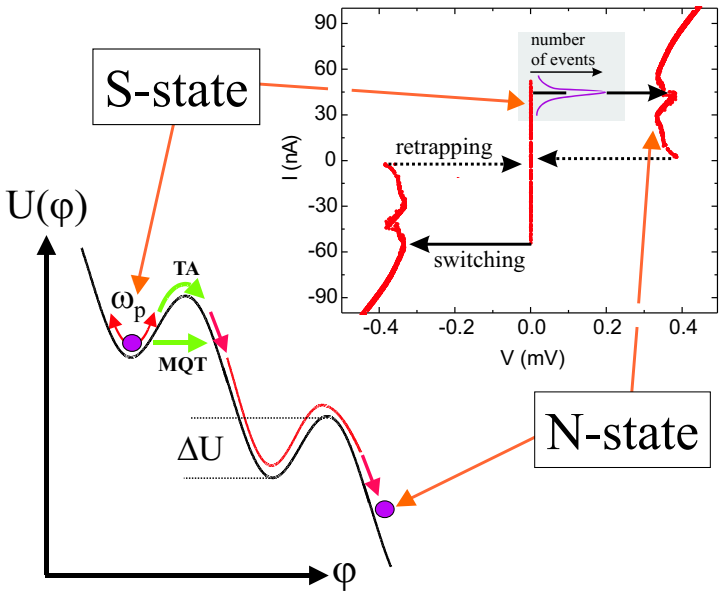

Figure 2. Dynamics of a hysteretic Josephson junction. The top frame presents an example of a measured IV-characteristic. In the superconducting state (S-state) the phase mainly oscillates in the well and the average voltage is close to zero. The phase particle can escape from well either by thermal activation (TA) or macroscopic quantum tunnelling (MQT) and the system switches to the free running state (N-state). In the N-state the voltage across the junction is approximately twice the superconducting gap ($2\Delta_{Al} \approx 360\,\mu$V). The escaping is stochastic process and by sweeping the current repeatedly one can measure the distribution of the switching currents (inset in the IV-characteristic figure). In this work we used a pulse technique, which yields the integral of this distribution directly.

probability in a measurement with a set of current pulses with fixed amplitude and duration, determining the statistical probability of junction to switch into a high voltage free running state. Usually one is measuring the switching probability as a function of current pulse amplitude $P(I)$, which yields *cumulative histograms* of switching currents (see Fig. 8).

2.3. The effects due to frequency dependent Q

In a typical experimental setup the junction is also capacitively shunted by the stray capacitance of, *e.g.*, the leads, besides by the junction capacitance. A more realistic equivalent circuit of the junction is thus that presented in Fig. 1 (c) instead of the simple RCSJ-model of (b). At low frequencies the dissipation is mostly determined by the junction subgap resistance, which is usually of the order of 1 MΩ, but at high frequencies, *e.g.*, at ω_p, the impedance is typically small because C_s is a short and R_s is small. In the S-state the phase mainly oscillates in a well at plasma frequency and it may transit from a well to another in a time which is of the order of the inverse plasma frequency. The dissipation is thus characterized by $R(\omega_p)$ in this case. Without

specially designed environmental circuit this high frequency dissipation is usually of the order of vacuum impedance $Z_0 = \sqrt{\mu_0/\epsilon_0} \approx 377\,\Omega$. Yet after transition into the N-state the dominant part of dissipation takes place at low frequencies. Thus the junction can have very large Q at low frequencies with very small retrapping current, yet in the supercurrent branch the junction can be overdamped [14, 15].

2.4. dc-SQUID

A dc-SQUID consists of a superconducting loop and two weak links. In the limit of small loop inductance L_{loop} ($\beta_L \equiv \frac{2\pi L_{loop} I_c}{\Phi_0} \ll 1$ [9]), the potential energy of the dc-SQUID can be written as

$$U_J(\gamma) = E_J\sqrt{2(1+\delta^2) + 2(1-\delta^2)\cos(\frac{2\pi\Phi}{\Phi_0})}\ \cos(\gamma), \tag{3}$$

where γ is the phase across the dc-SQUID, Φ is the magnetic flux through the loop and δ determines the asymmetry of the dc-SQUID ($E_{J1,J2} = E_J(1 \pm \delta)$). The supercurrent ($I_{sc} = \frac{2e}{\hbar}\ \partial U_J/\partial\gamma$) can in this case be written as $I = I_c^0\sqrt{2(1+\delta^2) + 2(1-\delta^2)\cos(\frac{2\pi\Phi}{\Phi_0})}\ \sin(\gamma)$. Hereafter we will consider $\delta = 0$. Then we can write $I = I_c\sin(\gamma)$, where $I_c = 2I_c^0 \mid \cos(\pi\Phi/\Phi_0) \mid$. The potential energy of the dc-SQUID has also an inductive contribution due to the inductance of the dc-SQUID loop. However if the Josephson inductance $L_J = \Phi_0/2\pi I_c$ is much larger than the loop inductance ($\beta_L \ll 1$), this term is not affecting the dynamics and we can neglect it [16]. In an ideal case the dc-SQUID is a tunable single junction with maximum critical current twice that of one junction in the loop ($\delta = 0$). Both our dc-SQUIDs are in the $\beta_L \ll 1$ limit.

2.5. Current threshold detection using Josephson junctions

Schematical examples of circuits used in a current threshold detection are presented in Fig. 3 (a) and (b). In these set-ups, the goal is to measure the current induced by a generic current source. This current is called I_x. The thick blue lines indicate the superconducting parts of the circuits and the principle difference between circuits shown in (a) and (b) is that the circuit in (a) can be used for measuring currents induced by externally *biased* circuits in contrast to (b), where the measured circuit is purely inductively shunted and it can be used for measuring a persistent supercurrent. The circuit presented in Fig. 3 (a) can be used in a conventional current measurement and it has also been proposed to be used, *e.g.*, in measurements of shot-noise [3, 4, 5]. In these measurements the JJ is providing the way to perform large bandwidth current measurements with extensive statistical averaging. The scheme presented in Fig. 3 (b) is similar to what has been used, *e.g.*, in the "Quantronium" experiment [1, 17, 18], but the circuit has also been proposed for measurements of quantum errors in Cooper pair pumping [19].

In both examples, (a) and (b), the measured current I_x runs in parellel with biasing current I_{bias} through the measuring junction (or a dc-SQUID as in Fig. 3). A

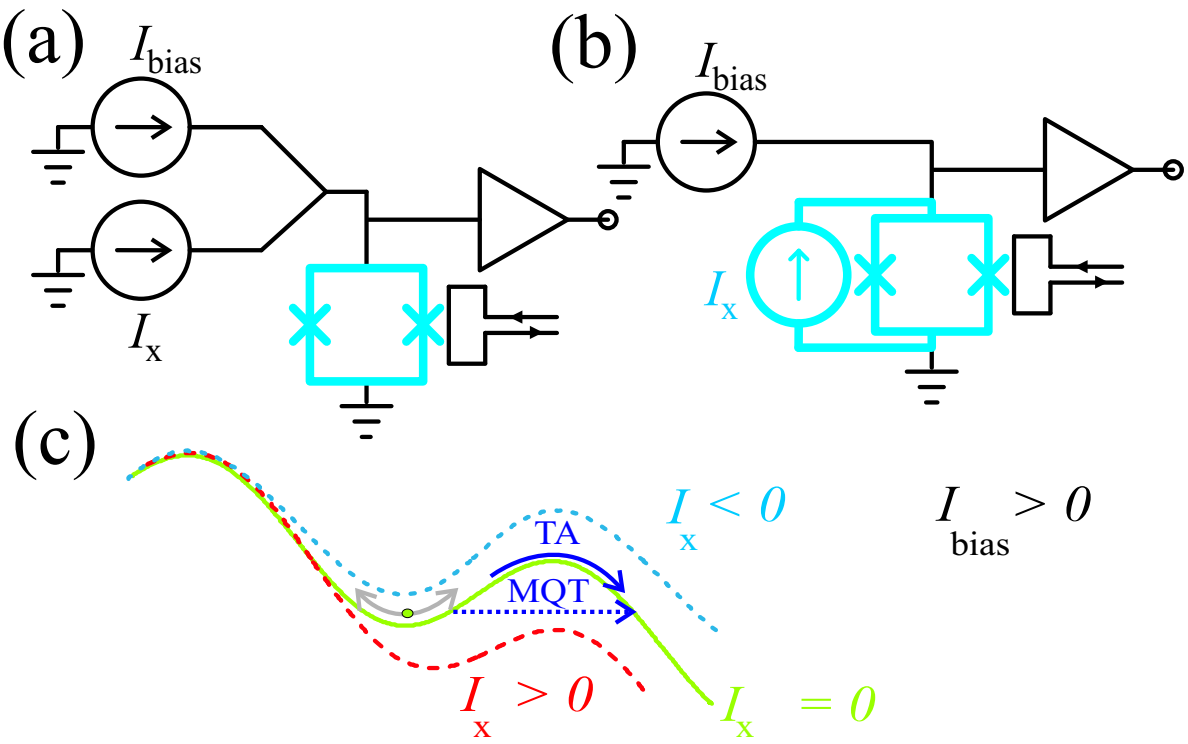

Figure 3. Schematical examples of current threshold detection using Josephson junctions or dc-SQUIDs. I_x is the current to be measured and I_{bias} is the biasing current. The thick blue lines indicate the superconducting parts of the circuit which measures I_x. (a) Circuit for a classical current probing. (b) Circuit for inductively shunted current measurements (*e.g.* Josephson junction circuits). (c) The schematic of the cosine potential at different values of current through the junction.

direct measurement can be obtained by measuring the corresponding change in escape probability for a constant I_{bias}. From this change I_x can be extracted. However the working point of the detector is not constant in this measurement, which can induce an error. A second measurement method is to regulate I_{bias} in order to keep the escape probability equal in the absence and in the presence of the signal to be measured. The current through the measuring junction is then equal in the two cases and loading errors, *e.g.*, the change of the Josephson inductance and superconducting phase, can be neglected. I_x is then directly given by the variation of I_{bias}.

The sensitivity of the current threshold detection with constant bias current pulses can be defined as $S = dP/dI$ (the derivative of the cumulative histogram). In current measurements the resolution is $\delta I = \delta P/S$. With TA and MQT models the maximum of the sensitivity is reached with the current pulse amplitude, which corresponds approximately to the 70 % escape probability. In Fig. 4 we present the maximum sensitivity as a function of the critical current and capacitance, calculated by using TA and MQT models. We have not taken into account the small effect of dissipation. A single Josephson junction with fixed oxidation parameters is covering only a line on the (I_c, C) -plane in Fig. 4 with an almost constant sensitivity. For typical oxidation

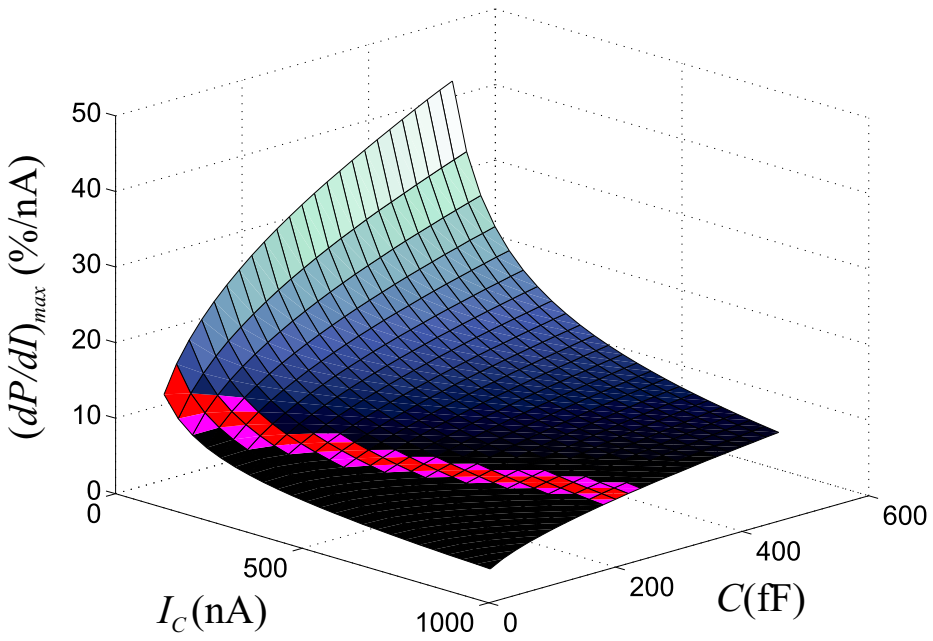

Figure 4. The maximum current sensitivity of an escape junction as a function of junction capacitance and critical current at $T = 25$ mK calculated by using a combination of TA and MQT models. The effects of dissipation have not been taken into account. The red region indicates the regime for a single Al-AlOx-Al tunnel junction with typical oxidation parameters resulting in 1 k$\Omega(\mu\text{m})^2$ and 50 fF$/(\mu\text{m})^2$ specific resistance and capacitance, respectively.

parameters of Al-AlOx-Al junctions this is presented as a red region. We have used the values 1 k$\Omega(\mu\text{m})^2$ and 50 fF$/(\mu\text{m})^2$. By decreasing junction area, both critical current and junction capacitance are decreasing. However the sensitivity $(dP/dI)_{max}$ remains fixed. Therefore it is beneficial to use a dc-SQUID configuration instead, where one can tune the critical current and capacitance independently and thus increase sensitivity remarkably.

The number of switching events is binomially distributed, whereby we find that the standard deviation of the measured escape probability is

$$\delta P = \frac{\sqrt{P(1-P)}}{\sqrt{N_{tot}}}, \tag{4}$$

where P is the measured escape probability and N_{tot} is the total number of current pulses on the measurement. The maximum of dP occurs at $P = 0.5$ and it vanishes at $P = 0$ and at $P = 1$. The current resolution is thus not the best at the current value where the maximum sensitivity is reached, but at a probability, which is a slightly higher instead ($P \simeq 0.8$).

Table 1. The parameters of the measured samples. Both the critical current I_c (Ambegaokar-Baratoff value calculated from the normal state resistance [9]) and the sample capacitance C_J [calculated based on the junction area and 50 fF/(μm)^2] are given for the whole tunable circuit in case of dc-SQUID samples.

sample	R_n (kΩ)	I_c (nA)	E_J (K)	C_J (fF)	$\omega_p^0/2\pi$ (GHz)
intermediate coupling					
SQ1	1.3	199	4.6	100	12.2
JJ1	0.41	630	14.5	130	19.0
weak coupling					
SQJJ					
single junction	11.6	23.4	0.53	30	7.5
dc-SQUID	3.8	74.5	1.7	50	10.5

3. Experimental details and measured samples

The parameters of the measured samples are presented in Table 1. All the measured samples were made out of aluminum and they were fabricated using standard electron beam lithography and aluminum metallization in a UHV evaporator. The AlOx tunnel barriers were formed by basic room temperature oxidation.

We report on measurements of three different samples: two with intermediate coupling energy ($E_J > k_BT$) and one with small coupling ($E_J \simeq k_BT$). Sample SQ1 has a conventional dc-SQUID geometry, which consists of two wide superconducting planes connected with two short superconducting lines with tunnel junctions in the middle forming the dc-SQUID loop of area 20×39 (μm)^2 (see Fig. 5). The purpose of wide planes was to reduce loop inductance, and the measured value was around 120 pH, which was small as compared to the calculated Josephson inductance ($L_J = \Phi_0/2\pi I_c = 3.2$ nH per junction). The dc-SQUID sample can thus indeed be considered as a single Josephson junction, whose I_c can be tuned. The loop inductance was estimated from the measured resonant voltage determined by C_J and loop inductance [20]. Sample JJ1, also with intermediate Josephson coupling, was a single junction between long inductive biasing lines.

The schematic of the sample with low coupling energy, SQJJ, is presented in Fig. 10. The sample consists of a single tunnel junction, a dc-SQUID and a long inductive line connected together in the middle. We assumed that the dc-SQUID is providing the tunable environment for the single junction. The distance between a dc-SQUID and a single junction was approximately 100 μm and a long inductive line was connected in between for separate biasing. The length of the line was around 2.5 mm leading to an inductance of $\sim l\mu_0 \approx$ 3 nH.

The schematic of the experimental setup is presented in Fig. 5. Measurements were done in dilution refrigerators with minimum temperatures around 20 - 30 mK. The refrigerators were equipped with strongly filtered lines (Thermocoax® and π-filters).

Switching probabilities have been measured by applying a set of short trapezoidal current pulses through the sample and by measuring the number of resulting voltage pulses. The statistical switching probability is thus simply $P = \#V\text{pulses} \,/\, \#I\text{pulses}$. Current pulses were created by applying voltage pulses either from the PC data aqcuisition card or from Agilent 33220A function generator through a large (100 kΩ -10 MΩ) resistor. Voltage across the sample was amplified and recorded by using the same data aqcuisition card. The normal delay time between current pulses was 500 μs, and it was measured to be long enough for cooling the sample after the dissipative switching event. For reducing flux noise we have used both superconducting lead and low temperature μ-metal shields in 4 K helium bath.

At the sample stage we used low pass RC-filters (surface mount components near the sample) as presented in Fig. 5. We use 4-wire configuration in all measurements, and thus there were 2 RC-filters connected to each electrode of the samples. In the measurements on a samples JJ1 and SQJJ we used surface mount capacitors (C_s = 680 pF), but in the measurements on sample SQ1 we had π-filters in series with resistors, with $C_s \sim 5$ nF capacitance to ground. The resistors were $R_s = 500\ \Omega$ in the measurements on SQ1 and 680 Ω in the measurement on samples JJ1 and SQJJ. The sample was connected to filters by ultrasonic bonding. The inductance of the bonding wires is of the order of nH, but the accurate value is not known. The agreement between theory and experiments (descibed below) is good by assuming that the inductive reactance is negligible at frequencies close to plasma frequency ($f_p = \omega_p/2\pi = 1{-}10$ GHz with current bias, see Table 1).

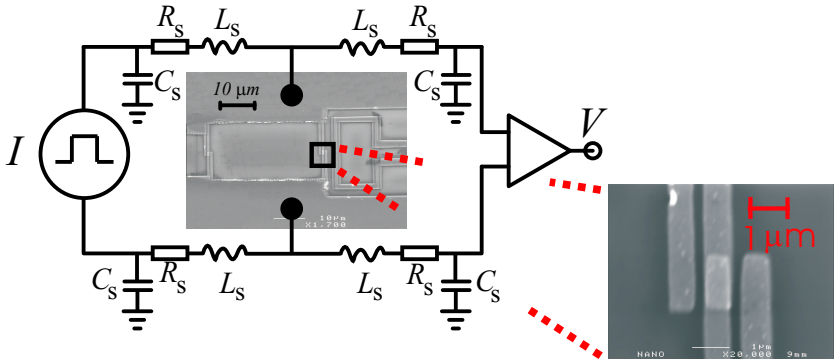

Figure 5. The schematic of the experimental setup for escape measurements and the electron micrograph of sample SQ1. The lower right corner of the figure presents the close-up of the tunnel junction. We use RC-filters at the sample stage. In the measurements on samples JJ and SQJJ the resistors close to sample R_S were 681 Ω and the value of the shunting capacitors C_S was 681 fF. In the measurements on a sample SQ1 we have $R_S = 500\ \Omega$ and $C_S \approx 5$ nF. In the case of sample SQ1 we also had a 20 kΩ resistor in parellel with voltage amplifier, to speed up the retrapping.

4. Josephson junctions with intermediate coupling

With decreasing critical current, the simple picture based on TA and MQT to explain the switching from the zero-voltage S-state to the free running N-state fails when E_J is comparable to $\hbar\omega_p$ or k_BT [21]. The first condition is due to the small number of quantized energy levels inside the well in this limit and thus the continuum approximation is not valid anymore. The latter one is explained by a change in the escape dynamics due to dissipation effects. Typically for a 500 Ω environmental impedance these effects occur for $E_J \leq 10k_BT$ which defines the condition of intermediate coupling.

4.1. Phase diffusion regime

In the S-state the voltage across the junction is not necessarily exactly zero, because phase can have 2π-slips, which causes a small average voltage across the junction. This phase diffusion is a dissipative process and therefore it can be harmful in applications where the junction is used *e.g.* as a quantum state detector.

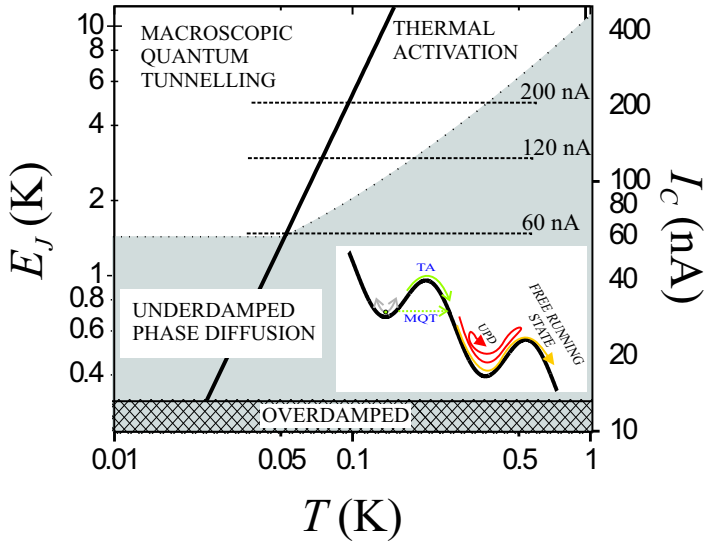

Figure 6. The different operation regimes of a small Josephson junction [21]. The thick black line shows the cross-over temperature between thermal activation and macroscopic quantum tunnelling regimes. The white area shows the regime where the conventional escape into a resistive state dominates (with current pulses of $\sim 100\ \mu$s length and with $\sim 500\ \Omega$ shunting impedance). Inset: The cosine potential. The dynamics inside a well (upper well) and the schematic dynamics *after* leaving the upper well.

When critical current is decreasing, dissipation is starting to play a more important role. The quality factor which is proportional to $\sqrt{E_J}$ is decreasing with decreasing E_J. On the other hand the escape rate is significant in the range of currents where the barrier height is comparable to the thermal energy. For strong coupling junctions, $E_J \gg k_B T$, this is the case when the bias current is only slightly below the critical current, but for small junctions this rate can be large even *without* tilting the cosine potential at all (I/I_c=0). At small critical currents the successive barrier tops are thus close in energy after escaping. If escape occurs at small enough currents, there is a non-zero probability that it will be followed by immediate relocalization to the *next* minimum due to dissipation. In this process the phase is diffusing from one well to another even though the junction can be underdamped and thus hysteretic. The maximum biasing current when this diffusion occurs can be given as [21]

$$I_m = \frac{4}{\pi Q} I_C, \tag{5}$$

where the value of Q corresponds to damping at plasma frequency ω_p. Below I_m the phase can be localized again and the voltage rise per one escape event is negligibly small and we are not able to count these events in a switching probability measurement, nor can we measure the average voltage due to these rare 2π phase-slip events.

The behaviour of the junction at a different values of E_J and T is described by the phase diagram of Fig. 6. The white area describes the region, where switching to the N-state after escaping is certain and thus the measurements of the escape dynamics are possible. The shaded area in this figure presents the phase diffusion regime, where escaping does not necessarily lead to a transition into the running state with 100 μs current pulses and with 500 Ω environmental impedance (C_J= 100 fF). This area is here divided in two different regimes: to underdamped ($Q > 1$) and overdamped ($Q < 1$) phase diffusion regimes. In contrast to underdamped phase diffusion (UPD), where the phase has to localize in the succeeding minimum, in overdamped phase diffusion regime the phase can slide down the potential with almost constant velocity.

4.2. Energy level quantization

For low lying energy levels the potential is close to the harmonic one and the level energies are $E_n \approx \hbar\omega_p \ (n + \frac{1}{2})$. The number of quantized energy levels inside the potential well can be approximated by $N = \sqrt{E_J/2E_c}\ (1 - I/I_c)^{5/8}$. For example in a 1 $(\mu\text{m})^2$ Al-AlOx-Al junction with usual oxidation parameters there are of the order of 10 levels at zero bias and this number is decreasing strongly with increasing bias current. In this case the basic continuum approximations do not hold anymore and more adequate models should be used. We take into account level quantization using the model of Larkin and Ovchinnikov [22, 23]. The scheme of the model is presented in Fig. 7. This semiclassical model takes into account the influence of the shape of the potential.

The total escape probability is calculated using $P_{esc}(\tau) = 1 - \sum_k \rho_k(\tau)$, where $\rho_k(\tau)$

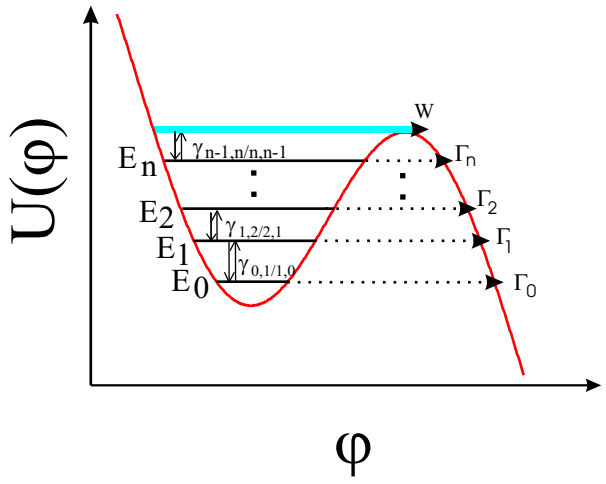

Figure 7. The dynamics inside a well. The model takes into account the anharmonicity of the potential. The model of the dynamics considers the transitions between the nearest neighbouring levels and the escape out of these levels.

is the probability of finding the particle in level k after the current pulse of length τ. The kinetic equation of the phase particle can be written as $\frac{d\rho_k}{dt} = \sum_j(\gamma_{kj}\rho_j - \gamma_{jk}\rho_k) - \Gamma_k\rho_k$. Due to the nearly parabolic shape of the potential the model takes into account only the transitions γ_{kj} between the nearest neighbouring levels and the tunnelling out, Γ_k. The relaxation rate between levels j and $(j-1)$ are well approximated by equation $\gamma_{j-1,j} = j\omega_p/4Q$. We also assume detailed balance: $\gamma_{j,j-1}{=}e^{-\beta(E_j-E_{j-1})}\gamma_{j-1,j}$. The positions and escape rates are calculated using the results in Ref. [22].

For calculating the full dynamics properly, nonlocalized states above (but close to) the barrier top must be included in the model as well. Actually, also the states just below the barrier ($E > \Delta U - 0.4\hbar\omega_p$) must be calculated in a similar manner. The expressions for calculating the shape of these broad levels is given in the Ref. [22].

The final state $\overline{\rho} \equiv [\rho_1\ \rho_2\ \ldots\ \rho_k]$ is calculated by numerically integrating the equation $N(\tau) = \frac{1}{\tau}\int_0^\tau e^{\mathbf{A}(t)}N(0)dt$, where

$$\mathbf{A} = \begin{pmatrix} -(\gamma_{0,1}+\Gamma_0) & \gamma_{1,0} & & \\ \gamma_{0,1} & -(\gamma_{1,0}+\gamma_{1,2}+\Gamma_1) & \gamma_{2,1} & \\ & \gamma_{1,2} & \ddots & \gamma_{n,(n-1)} \\ & & \gamma_{(n-1),n} & -(\gamma_{n,(n-1)}+\Gamma_n) \end{pmatrix} \quad (6)$$

is the tridiagonal transition matrix including all the transition elements. The current bias is set to zero in the beginning, and the initial state $\overline{\rho}(0)$ is Boltzmann distributed.

The possibility that the phase particle can relocalize in the succeeding well after tunnelling must be taken into account in the model as well. The dissipated energy in transition from one well to another can be approximated by $E_d \approx 8E_J/Q$ and by using that and the fact that the energy difference between the two successive maxima

is $-2\pi E_J I/I_c$, we can write that the level energy E must fulfill the condition

$$\Delta U - E < E_J\,(2\pi I/I_c - 8/Q) \tag{7}$$

to secure switching into the N-state. If condition (7) is not fulfilled, tunneling rate at that energy level is set to zero in the model. This means that in the next well the thermal distribution is reached immediately. With the low Q values in the experiment, the phase relaxes in the next well in a time $\sim \omega_p^{-1} \sim 100$ ps, which is far shorter than the typical time interval between phase diffusion events with studied current bias values (10...100 μs), and the assumptions of zero tunnelling rate and immediate recovery to the Boltzmann distribution in the next well are thus valid. Note that Eq. (7) gives the same threshold as Eq. (5) for the special case $\Delta U = E$, but in Eq. (7) we have taken into account the fact that after tunnelling the energy of the phase particle is not necessarily that at the potential maximum.

4.3. Results

In Fig. 8 we present the measured cumulative switching histograms (open circles) of sample SQ1 at different fluxes and temperatures. If we assume that the two junctions in the dc-SQUID are identical, we can infer that the corresponding critical currents at the lowest temperature are $I_c(\Phi) = 200$ nA, 128 nA and 55 nA, at $\Phi/\Phi_0 = 0$, 0.28 and 0.41 respectively. The measurements were done both at the negative and positive values of flux in order to make sure that the external flux did not change during the measurements. The number of repetitions was 10^4 and the length of the current pulses was 200 μs. In the measurement of sample JJ1 we use 10 ms current pulses and the number of repetitions was 200.

4.3.1. The different operation regimes of samples In Figs. 9 (a) and (b) we show measured histogram positions $I_{50\%}$ [$P(I_{50\%}) \equiv 0.5$] and widths ΔI ($\equiv I_{90\%} - I_{10\%}$) of samples SQ1 and JJ1. The position is normalized by the corresponding critical current. We also present the results of the basic TA and MQT model simulations. The weak effect of dissipation on MQT and TA rates was not included in the simulations. At low T all the measured data are consistent with MQT results. On increasing the temperature the parameters are constant up to the estimated cross-over temperature T_0. Above this the width is increasing and the position is moving down as TA model predicts. The qualitative agreement is good for most of the results up to a temperature, which we denote T_D. At T_D ΔI starts to decrease abruptly and the position of the histogram saturates. The dc-SQUID data measured at $\Phi = \pm 0.41\Phi_0$ are not following the simple theory even at low temperatures, since $T_D \leq 30$ mK in this case.

In the diagram of Fig. 6 we also present the critical current of SQ1 at fluxes 0, $\pm 0.28\Phi_0$ and $\pm 0.41\Phi_0$ by horizontal dashed lines. The phase diagram was calculated assuming a realistic shunting impedance $R(\omega_p) \simeq 500\ \Omega$ (the value of the surface mount resistors). It can be seen that the intersections of the dashed lines and the boundary of the phase diffusion regime are very close to the experimentally determined temperatures

T_D. The cross-over from thermal escape into underdamped phase diffusion regime is thus causing the re-entrant steepness of the histograms.

At the temperature T_D the position of the sample SQ1 histograms is saturating at about the same value $I \simeq 0.35 I_c$ at all magnetic fluxes (JJ1 at $I \simeq 0.3 I_c$). If we assume $R(\omega_p) \simeq 500\ \Omega$, we obtain $Q \approx 4$ ($I_c = 200$ nA and $C_J = 100$ fF), which yields indeed

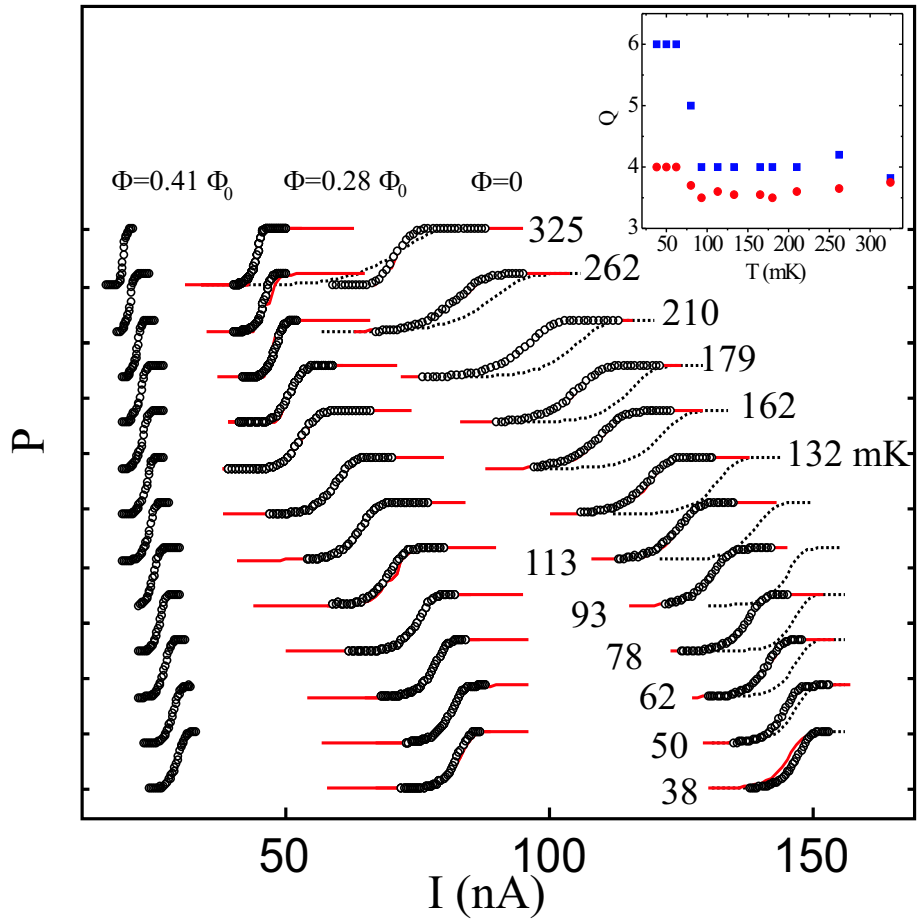

Figure 8. Cumulative histograms of the dc-SQUID at different temperatures. The rightmost curves are measured at zero field and in the left and in the middle we present histograms measured at $0.41\Phi_0$ and $0.28\Phi_0$ respectively. The curves are shifted for clarity and the vertical spacing between ticks corresponds to escape probability of unity. Solid red lines are from simulations based on Larkin and Ovchinnikov model [22, 23] described in the text and black dotted lines show the results of the basic model where MQT and TA rates are added together. Inset: The blue squares and red circles are the fitted quality factors at different temperatures at zero flux and $\Phi = 0.28\Phi_0$, respectively. The number of repetitions at each current, N_{tot}, was 10^4 and the length of the current pulses was 200 μs.

$I_m \simeq 0.35 I_c$ through Eq. (5) like in the experiment. In the case of a single junction $R(\omega_p) \simeq 681\ \Omega$ gives $Q \approx 13$ yielding $I_m \approx 0.1\ I_c$ instead of the measured $0.3\ I_c$. The latter current would rather correspond to $R(\omega_p) \simeq 230\ \Omega$ giving $Q \approx 4$ and an estimated $T_D = 700$ mK which is consistent with the measurements.

In chapter *2.4* we discussed the sensitivity of the Josephson junction threshold detection characterized by the steepness of the cumulative histograms. In the underdamped phase diffusion regime, however, the re-entrant steepness is due to missed escape events and relocalisation, and it might be harmful in some detector applications, where dissipation is to be avoided.

4.3.2. The effects due to finite number of quantized energy levels In Fig. 8 we present results of both the simulations with quantized energy levels (QEL) and dissipation (solid red lines) and with basic TA-MQT model (dotted line). The results of the TA-MQT model are presented only for data measured at zero flux. Figure 8 shows that the plain TA-MQT models cannot account for our observations. Except for the data at the lowest temperatures the width and the position of the measured histograms deviate from the simulated ones (dotted line). Dissipation alone cannot explain the difference. The basic TA model yields $\Delta I \propto T^{2/3}$ [10] and it can be seen in Figs. 8 and 9 that the dc-SQUID has weaker temperature dependence even well below T_D. In these samples there are just few energy levels in the well and thus the assumptions of continuous energy spectrum are not valid here [10]. We present results of QEL-model simulations for data at zero and $\pm 0.28\Phi_0$ fluxes. At $\pm 0.41\Phi_0$ I_c is so small that the escape probability is large

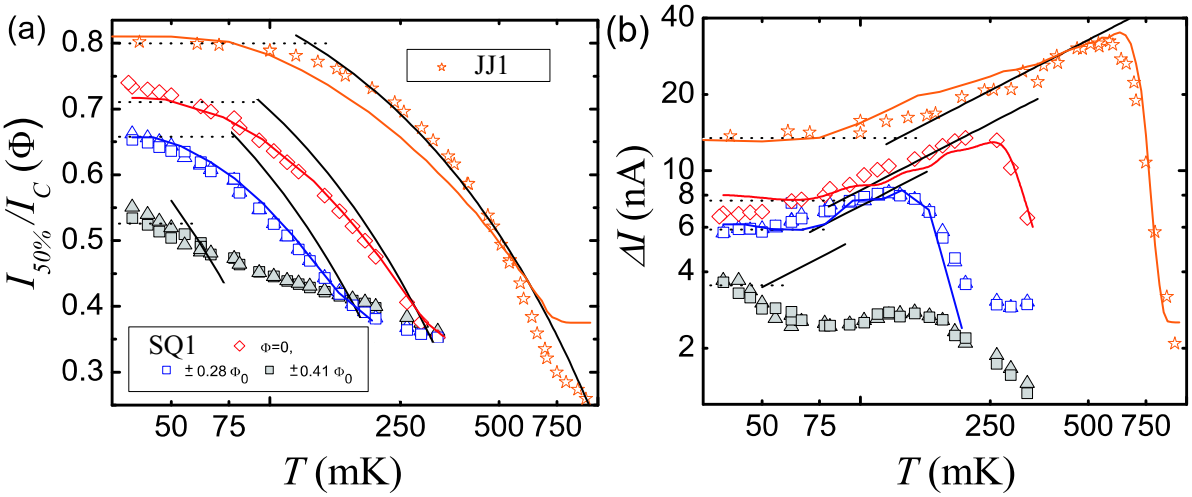

Figure 9. (a) The positions ($I_{50\,\%}$) and (b) the widths (ΔI) of the measured histograms. The position is normalized to the corresponding calculated critical current $I_c(\Phi)$ at $T = 0$. For non-zero fluxes we present data measured at both positive and negative values of flux. Black solid and dotted lines are results (with known junction parameters) of thermal activation and macroscopic quantum tunnelling model, respectively, ignoring dissipation. Blue, red and orange solid lines are the corresponding quantities from simulations based on Larkin and Ovchinnikov model.

even at zero bias (except at the lowest temperatures). This means that the phase is running constantly rather than infrequently escaping from well to another, and thus our model does not work anymore. The only fitting parameter was the quality factor Q, and the fitted values (presented in the inset of the Fig. 8) were in a very reasonable range. At $\Phi = 0$ we find $Q \approx 6$ at the lowest temperature, and it decreases with increasing temperature up to 4 at 325 mK. At $\Phi = \pm 0.28\Phi_0$ $Q \approx 3...4$, again decreasing with temperature. The agreement between simulation and measurements is excellent. The position and the width of the measured histograms coincide and, in particular, at higher temperatures the simulated histograms also start to get steeper again. At higher temperatures the upper energy levels, whose escape rate is significant with smaller potential tilting angles, are populated as well. The histograms thus peak at smaller currents and the condition of Eq. (7) is not necessarily fulfilled anymore. Dissipation is screening part of the events and the histogram gets distorted. What remains in the measured (and simulated) histograms is the escape from the levels at the tail of the Boltzmann distribution above the dissipation barrier. The measured samples can thus be tuned from pure escape regime deep into phase diffusion by varying temperature and flux.

5. Josephson junctions with weak coupling

When the coupling energy E_J is of the order of k_BT, the escape rate is significant even *without* bias current. This means that the junction is dissipative also with zero bias. Figure 6 demonstrated that when $I_c < 60$ nA the system is in the phase diffusion regime even at the lowest temperatures with 500 Ω environmental impedance. The measured weak coupling junctions are thus not obeying simple escape dynamics from a metastable potential well into a free running state, but the escape occurs over a dissipation barrier instead. The measured histograms of both the dc-SQUID and the single junction of sample SQJJ (data not shown here) indeed show qualitatively similar behaviour as what is presented in Fig. 9 (a) and (b) at $\Phi = \pm 0.41\Phi_0$.

5.1. Zero-bias resistances

Predominantly unshunted hysteretic junctions can be overdamped due to frequency dependent environmental impedance [$R(\omega_p) \sim Z_0 \approx 377\ \Omega$]. This can be the case especially on the samples with small E_J, which usually means also small ω_p like in the sample SQJJ. Small coupling energy ($E_J \sim k_BT$) yields also to large escape rate and further to large phase diffusion rate. If the rate is large enough, the average voltage across the junction start to be measurable (but still $\ll 2\Delta/e$). In SQJJ, the escape rate of the single junction is large, *i.e.* the phase diffusion is strong, leading to a small measurable voltage ($\ll 2\Delta/e$) across the junction. Therefore the current-voltage characteristics present a finite slope even at zero current. Ingold et al. have shown that

for overdamped junctions this zero-bias resistance can be given as [24, 9]

$$R_0 = \frac{R}{\mathrm{I}_0^2[E_J/k_BT] - 1}, \tag{8}$$

where I_0 is the modified Bessel function and R is a shunting impedance.

The zero-bias resistances R_0 due to phase diffusion of both the single junction and the dc-SQUID are plotted at different temperatures by using lock-in technique in Fig. 11. They are fitted by the predicted resistance given by Eq. (8) using $R = 270\ \Omega$ as a fit parameter. The theory closely follows the measurement over two decades in resistance. The measurement noise level sets the minimum measurable resistance to somewhere around $10\ \Omega$ which corresponds to the flat background in Fig 11 (a) and 11 (b). R_0 of the dc-SQUID was also measured at different magnetic fields [Fig 11 (a)].

We observe that R_0 can be tuned by changing magnetic flux inside the dc-SQUID. The zero-bias resistance is increasing strongly with decreasing critical current as Eq. (8) predicts. With critical currents of the order of 10 nA, R_0 is larger than $10\ \Omega$ even at the lowest temperatures.

5.2. Tunable environment

Escape from the phase diffusion branch to the running state is a complicated process and it does not have similar simple analytical expressions as, *e.g.*, the basic thermal activation has. Yet this thermally activated process is strongly environment dependent as our Monte Carlo simulations, based on Refs. [14, 15], clearly demonstrate. Turlot

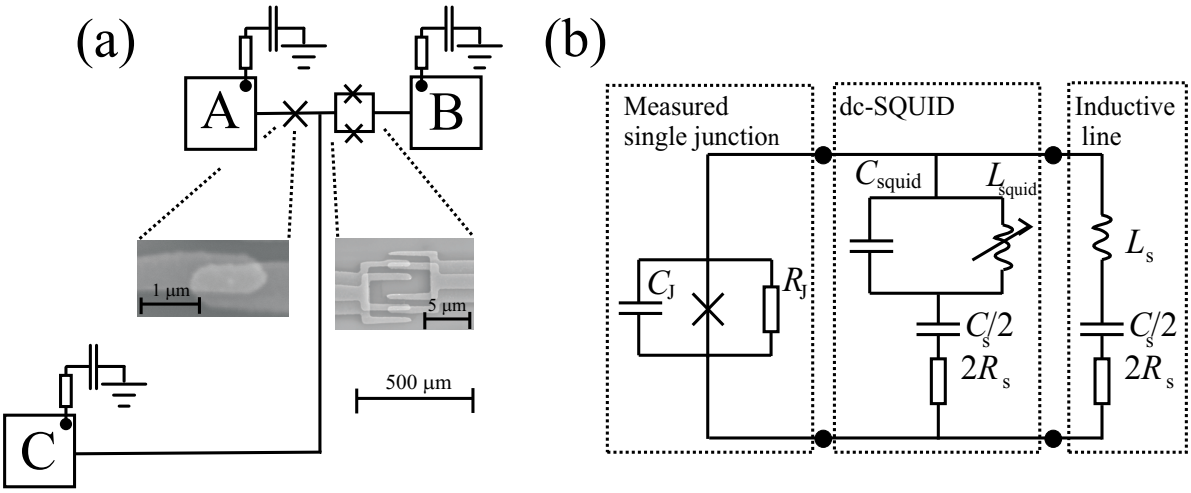

Figure 10. (a) Schematics of the sample SQJJ with tunable environment and micrographs of the junctions in this sample. The distance between the single junction and the dc-SQUID is about $100\ \mu$m. In the actual measurement we use 4-wire configuration and there were thus 2 RC-filters connected to every electrode. The value of the capacitors to ground was 680 pF for one filter, and the resistors were $680\ \Omega$ each (the actual high frequency shunting resistance to ground was thus $\approx 340\ \Omega$). (b) Circuit model of sample SQJJ.

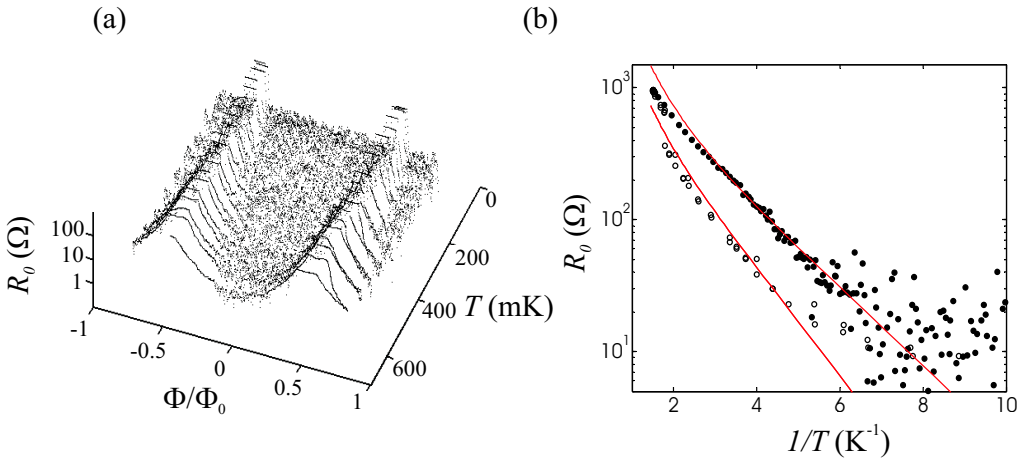

Figure 11. (a) The zero-bias resistance R_0 of the dc-SQUID of sample SQJJ at different magnetic fields and temperatures. The measurement noise level sets the minimum measurable resistance to about 10 Ω (the flat region). The saturation to 250 Ω close to half of flux quantum is due to the saturation of the lock-in amplifier. (b) Filled circles are the R_0 of the dc-SQUID of sample SQJJ at $\Phi = 0.42\,\Phi_0$ at different temperatures. Open circles presents the similar results on the single junction of sample SQJJ. Lines are the results of the model for overdamped junctions [Eq. (8)] assuming the same fitted value 270 Ω of shunting in both cases. E_J of the dc-SQUID was estimated from the flux value and the normal state resistance, and assuming a symmetric structure.

et al. have measured how thermally activated escape rate over a tilted cosine potential barrier varies with changing impedance of the frequency dependent environment [25]. It was shown in their work that if $1/Re\{\mathrm{Y}(\omega)\}$ does not vary too rapidly close to plasma frequency, the dominant part of the dissipation happens in the vicinity of ω_p [25, 26]. With frequency dependent environment the thermal activation rate Γ_{TA} thus approximately varies like $1/Re\{\mathrm{Y}(\omega_p)\}$ with changing impedance [Eq. (1)].

In this work we measured the dynamics of escape from the phase diffusion regime to the free running state by varying environmental impedance. The escaping rate follows a similar Arrhenius law

$$\Gamma_{TA}^{PD} = a_d e^{-(U_s - U_i)/k_B T}, \tag{9}$$

as the standard thermal activation, but now escape occurs over a dissipation barrier $U_s - U_i$ instead (s corresponds to a saddle point and i to the initial state) [6]. The prefactor a_d is similarly a dissipation dependent parameter as a_t for thermal activation over cosine potential barrier [Eq. (1)]. We thus assume that the escape rate Γ_{TA}^{PD} from the phase diffusion regime varies also like $1/Re\{\mathrm{Y}(\omega_p)\}$.

In our sample the environment presented by the dc-SQUID on the single junction, and vice versa, are strongly inductive. The Josephson inductance of the dc-SQUID at zero field is of the same order of magnitude ($L_J \approx 4.5$ nH) as the inductance of the long line, but it is increasing strongly with increasing magnetic field. We consider the dc-SQUID here as a tunable environmental inductance of the single junction and measured

how changing the Josephson inductance of the dc-SQUID is affecting escape dynamics of the single junction.

The sample is approximated by an equivalent circuit presented in Fig. 10 (b). In this model the dc-SQUID is approximated by a parallel combination of Josephson inductance and junction capacitance similarly as Warburton *et al.* successfully did with high-T_c intrinsic Josephson junctions [27]. We have not taken into account the fact that close to $\Phi = 0.5\Phi_0$ the dc-SQUID is also in the dissipative phase diffusion regime, which might affect escape dynamics. The parallel resistance of the dc-SQUID is assumed to be large. Notice that this does not mean that the dissipation that the dc-SQUID can see at *high frequencies* is small. The capacitance C_s= 10 pF is assumed to be the sum of capacitances of the surface mount capacitors and of the stray capacitances of the line. The high frequency dissipation is modeled with resistance R_s, which is most probably close to the value of surface mount resistors ($\sim 340\ \Omega$) or to the value of vacuum impedance ($Z_0 \approx 377\Omega$). Figure 12 (a) presents the calculated real part of the admittance of the model environment of the single junction which corresponds to the dc-SQUID with the inductive line (Fig. 10). In calculations we used the value 3 nH for the inductance of the long line and the parameters of the dc-SQUID are given in Table 1. The impedance is modified by changing the flux through the SQUID. The environmental admittance of the single junction at the attempt frequency ω_p is presented in Fig. 12 (b).

We measured the escape probability of the *single* junction as a function of flux through the dc-SQUID. In the measurement the current bias was fed through the single junction line (A electrode in Fig. 10) to the long inductive line (C) and the voltage was measured between these electrodes. At each temperature we first measured the amplitude of the current pulse, which corresponds to approximately 70 % switching probability at zero flux. We measured escape probability of the single junction as a function of flux at this fixed current amplitude. Results are presented in Fig. 12 (c) and the inset of Fig. 12 (c) shows $I_{70\%}$ at zero flux at each measuring temperature.

Figure 12 (c) shows that the measured escape probability indeed follows the general behaviour of the real part of the modelled environmental admittance at plasma frequency of the single junction plotted in Fig.12 (b) as was predicted above. We do not have a quantitative model for the flux dependence of the escape rate, but it is obvious that the dc-SQUID acts as a tunable environment for the single junction such that it can decouple the external noise at a certain value of flux. At $\Phi = 0$ the plasma frequency of the *dc*-SQUID is larger than that of single junction due to different thickness of the oxide barriers (see Table 1). In this case $Y(\omega_p)$ of the single junction presented by the dc-SQUID is large. With increasing flux, the plasma frequency of the *dc*-SQUID reduces. Around $\Phi = \pm 0.3\Phi_0$ it coincides with that a of single junction and environmental admittance is reduced and thus escape rate is significantly suppressed. The behavior is qualitatively the same at all temperature, but at higher temperatures the escape rate is strongly enhanced close to $\Phi = \pm 0.5\Phi_0$. One possible explanation for this is that the phase diffusion in the *dc*-SQUID is playing a role, which is not taken into account in

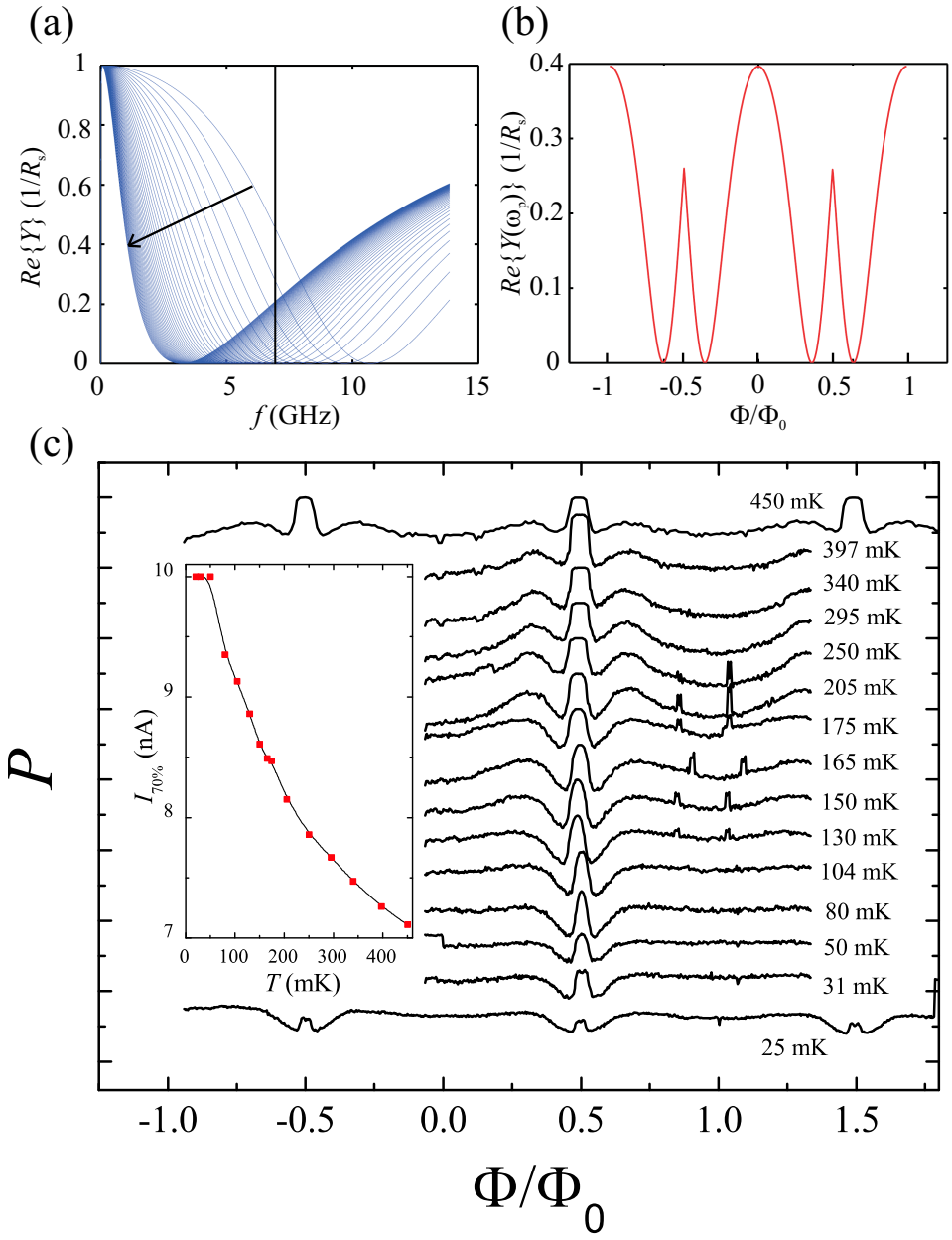

Figure 12. (a) The real part of the admittance $Re\{Y\}$ of the parallel combination of the dc-SQUID and of the inductive line of Fig. 10 as a function of frequency at different fluxes between 0 and Φ_0. The vertical line corresponds to the plasma frequency of the single junction at zero bias current. The arrow indicates the direction of increasing Josephson inductance. The calculations are done by using the value 3 nH for long inductive line and the parameters given in Table 1. (b) $Re\{Y\}$ as a function of flux at the plasma frequency of the single junction. (c) Measured switching probability of the *single* junction of sample SQJJ at constant current bias as a function of applied magnetic flux at several temperatures between 25 mK and 450 mK. Curves are shifted for clarity and the vertical spacing between ticks corresponds to escape probability of unity. Inset: The current, which corresponds to 70 % escape probability at various temperatures, as measured on the single junction of sample SQJJ.

our model. The flux dependence of the escape rate in the single junction suggests that dissipation in the zero voltage state takes place mainly at plasma frequency. Further, the dominant part of the dissipation is, in our case, physically happening far away from the junction and the quasiparticle resistance is not playing an important role.

6. Concluding remarks

Our measurements confirm that dissipation plays a more important role in the phase dynamics of Josephson junctions when the critical current decreases. The parameters of the measured samples were in the intermediate range, where the simple escape from a single metastable state, and phase diffusion both play a role. The sample with the smallest critical current consists of a single Josephson junction and a dc-SQUID close to each other, the latter of which acts as a tunable inductive protection for the single junction. We were able to study the effects of dissipation on escape dynamics by varying the temperature, flux and environment. The measurements with tunable environment show that escape from the phase diffusion regime depends strongly on the environment.

In summary, our observations show that in order to use junctions with $E_J \sim k_B T$ for current detection purposes, one should pay particular attention to the environmental circuit. With low Q values these junctions can be in the underdamped phase diffusion regime, which might be harmful in threshold current measurements. This regime is also dissipative, which is undesirable in some applications, *e.g.*, in the detection of quantum state of a superconducting quantum bit. Our measurements with tunable environment confirm that the inductive leads can provide a way to further decrease the critical current without losing the beneficial properties in threshold current measurements.

*N*ote added: since the submission of this manuscript, similar experimental results of additional cross-over from TA to underdamped phase diffusion were reported by Krasnov *e*t al. and by Männik *e*t al. [28]. Their interpretation differs from ours in details.

Acknowledgments

The Academy of Finland and EU IST-FET-SQUBIT2 are acknowledged for financial support. We are grateful to A. O. Niskanen, T.T. Heikkilä, and M. Paalanen for helpful discussions.

References

[1] D. Vion, A. Aassime, A. Cottet, P. Joyez, H. Pothier, C. Urbina, D. Esteve, and M.H. Devoret, Science **296**, 886 (2002).
[2] S. Saito, M. Thorwart, H. Tanaka, M. Ueda, H. Nakano, K. Semba, and H. Takayanagi, Phys. Rev. Lett. **93**, 037001 (2004).
[3] J. Tobiska and Yu. V. Nazarov, Phys. Rev. Lett. **93**, 106801 (2004).
[4] J.P. Pekola, Phys. Rev. Lett. **93**, 206601 (2004).

[5] J.P. Pekola, T.E. Nieminen, M. Meschke, J.M. Kivioja, A.O. Niskanen, J.J. Vartiainen, cond-mat/0502446 (2005).
[6] D. Vion, M. Götz, P. Joyez, D. Esteve, and M. H. Devoret, Phys. Rev. Lett. **77**, 3435 (1996).
[7] J. Sjostrand, J. Walter, D. Haviland, H. Hansson, and A. Karlhede, cond-mat/0406510 (2004).
[8] A. Franz, Y. Koval, D. Vasyukov, P. Müller, H. Schneidewind, D. A. Ryndyk, J. Keller, and C. Helm, Phys. Rev. B **69**, 014506 (2004).
[9] M. Tinkham, *Introduction to superconductivity, 2nd ed.* (McGraw-Hill, New York, 1996).
[10] U. Weiss, *Quantum Dissipative Systems*, (World Scientific, Signapore, 1999), 2nd ed.
[11] M. Büttiker, E.P. Harris, and R. Landauer, Phys. Rev. B **28**, 1268 (1983).
[12] E. Freidkin, P.S. Riseborough, and P. Hänggi, Z. Phys. B. **64**, 237 (1986).
[13] A.O. Caldeira and A.J. Leggett, Phys. Rev. Lett. **46**, 211 (1981).
[14] J.M. Martinis and R.L. Kautz, Phys. Rev. Lett. **63**, 1507 (1989).
[15] R.L. Kautz and J.M. Martinis, Phys. Rev. B **42**, 9903 (1990).
[16] F.Balestro, J. Claudon, J.P. Pekola, and O. Buisson, Phys. Rev. Lett. **91**, 158301 (2003).
[17] O.Buisson and F. W. J. Hekking, in *Macroscopic Quantum Coherence and Quantum Computing*, edited by D.V. Averin, B. Ruggiero, and P. Silvestrini (Kluwer, New York, 2001), p. 137.
[18] O. Buisson, F.Balestro, J.P. Pekola, and F.W.J. Hekking, Phys. Rev. Lett. **90**, 238304 (2003).
[19] R.Fazio, F.W.J. Hekking, and J.P. Pekola, Phys. Rev. B **68**, 054510 (2003).
[20] H.S.J. van der Zant, D. Berman, and T.P. Orlando, Phys. Rev. B **49**, 12945 (1994).
[21] J.M. Kivioja, T.E. Nieminen, J.P. Pekola, J.Claudon, O. Buisson, F.W.J. Hekking, and J.P. Pekola, cond-mat/0501383 (2005).
[22] A. I. Larkin and Yu. N. Ovchinnikov, Zh. Eksp. Teor. Fiz **91**, 318 (1986); A. I. Larkin and Yu. N. Ovchinnikov, Sov. Phys. JETP **64**, 185 (1987).
[23] A. I. Larkin and Yu. N. Ovchinnikov, Zh. Eksp. Teor. Fiz **87**, 1842 (1984); A. I. Larkin and Yu. N. Ovchinnikov, Sov. Phys. JETP **60**, 1060 (1984).
[24] G.-L. Ingold, H. Grabert, and U. Eberhardt, Phys. Rev. B **50**, 395 (1994).
[25] E. Turlot, D. Esteve, C. Urbina, J.M. Martinis, M. H. Devoret, Phys. Rev. Lett. **62**, 1788 (1989).
[26] H. Grabert and S. Linkwitz, Phys. Rev. A **37**, 963 (1988).
[27] P.A. Warburton, A.R. Kuzhakhmetov, G. Burnell, M.G. Blamire, and H. Schneidewind, Phys. Rev. B **67**, 184513 (2003).
[28] V.M. Krasnov *et* al., cond-mat/0503067; J. Männik *et* al., cond-mat/0503729.